

# Graphene Micromesh for Transparent Conductive Films Application

Ryousuke Ishikawa\*, Hirzoki Nishida, Hiro Fukushima, Sho Watanabe, Sohei Yamazaki, Gilgu Oh, Nozomu Tsuboi

Materials Science Program, Niigata University, 8050 Ikarashi 2-nocho, Nishi-ku, Niigata, 950-2181, Japan

\*Corresponding author: Tel: (+81)-25-262-6736. E-mail: ishikawa@eng.niigata-u.ac.jp

Received: 15 August 2018, Revised: 06 December 2018 and Accepted: 05 January 2019

DOI: 10.5185/amlett.2019.2238  
www.vbripress.com/aml

## Abstract

In order to improve the properties of the graphene transparent conductive film we developed a process of O<sub>2</sub> plasma patterning graphene using a metal mesh as an etching mask. The CVD growth conditions of high quality multilayer graphene samples consisting of 400 layers or more were found using Ni foil, and the  $R_{\text{sheet}} = 3.4 \pm 0.6 \Omega/\text{sq.}$  was achieved. The best performance of graphene micromesh based transparent conductive films so far was  $R_{\text{sheet}} = 22.2 \Omega/\text{sq.}$  at  $T = 47.1 \pm 1.9 \%$ . According to theoretical calculations based on combined resistance of the two-dimensional resistance lattice circuit, a combined resistance of  $46.8 \Omega$  can be realized at  $T = 90\%$ . Copyright © VBRI Press.

**Keywords:** Patterned graphene, plasma etching, micromesh, transparent conductive films, solar cells.

## Introduction

At present, indium tin oxide (ITO) is widely used as a transparent conductive film. However, indium, which is a raw material for ITO, is a valuable metal, and there is a limit to stable supply. On the other hand, graphene has high carrier mobility, high transparency, and it is composed only of carbon rich in raw materials, so it is promising as a transparent conductive film material [1-3]. In order to apply graphene as a transparent conductive film of a solar cell, the performance of graphene is not sufficient and further improvement is required. We have been attempting to improve the performance of graphene transparent conductive film by carrier doping so far and have established chemical doping technology using organic molecules such as 1,4-Bis(dicyanomethylene) cyclohexadiene (TCNQ) and bis(trifluoromethanesulfonyl) amide (TFSA), or molybdenum oxide which is a more stable inorganic material [4-7]. However, fabrication processes such as quantum dot solar cells require high-temperature heat treatment [8,9], and such doping techniques sometimes cannot be applied. Graphene-based film is useful as a transparent electrode material for devices requiring extremely high stability like space solar cells with ultra-high efficiency, particularly resistance to radiation and cryogenic environments [10]. Furthermore, the graphene-based film can also be applied to photo-electrochemical water splitting devices [11].

In this research, we aimed to improve the performance of the graphene film itself without using carrier doping. Specifically, we first developed a high quality multilayer graphene film with low sheet resistance ( $R_{\text{sheet}}$ ) even though it has a low optical

transmittance ( $T$ ), and tried to improve the transparency by patterning it. As a method of patterning graphene, a method of patterning a metal catalyst in advance [12] and a method of patterning by lithography and etching [13] have been proposed, but as a simpler method, we focused on a method of patterning graphene by plasma etching through a metal mask [14]. Previous reports on patterning of graphene are aimed at development of nano-devices by microfabrication and surface modification of graphene [15-18]. In this research, we aimed to establish a patterning technique using a metal mask specialized for improving characteristics as a transparent conductive film. We also discussed the theoretical analysis of the graphene micromesh by considering the resistance as the combined resistance of the two-dimensional resistance lattice circuit.

## Experimental

### Materials

The 50  $\mu\text{m}$  thickness of Ni foils (99 + %) as catalyst for graphene growth were purchased from Nilaco. A polymethyl methacrylate (PMMA; Sigma-Aldrich, average  $M_w \sim 996,000$ ) was dissolved in chlorobenzene (Wako Pure Chemical Industries) with a concentration of 46 mg/mL. Several stainless steel metal meshes (ESCO, SUS304) with different mesh sizes were used as the etching masks. Mesh size is defined by line width (W) and pitch (P) as shown in (Fig. S1). The mesh number indicates number of meshes in 1 inch (e.g. #20 means 20 meshes in 1 inch).

### Material synthesis

Graphene was synthesized using a thermal CVD system [19]. The 25 mm × 25mm of Ni foils were putted into the CVD furnace, and multilayered graphene films were synthesized using H<sub>2</sub> and CH<sub>4</sub> gas under the conditions shown in (Fig. S2).

After a PMMA protection layer was spin coated on the fabricated graphene films, Ni foil was etched away by FeCl<sub>4</sub> (3 M) solution [20]. The floated graphene films on the etchant were transferred onto soda lime glass and rinsed a few times with deionized water. Finally, the PMMA protection layer was removed by acetone.

The schematic image of graphene micromesh fabrication process is shown in (Fig. 1). The metal mesh mask was putted on the transferred graphene films, then introduced into the plasma chamber. After evacuation, pure O<sub>2</sub> was introduced up to 50 Pa, and patterning was carried out by irradiating RF plasma of 50 W input power for 15 minutes.

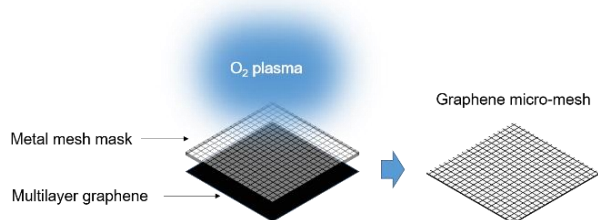


Fig. 1. Schematic image of graphene micromesh fabrication process.

### Characterizations

The quality of graphene samples were analyzed by Raman spectrometer (JASCO, RMP-510). The patterned graphene films were evaluated for its optical transmittance by UV-Vis spectrum measurement (JASCO, ARSN-733) and sheet resistance by Hall-effect measurements and van der Pauw's method (ECOPIA, HMS-5000). The surface morphology was observed using scanning electron microscope (SEM; JEOL, JCM-6000).

### Results and discussion

The results of evaluating the electrical and optical properties of the multilayer graphene films on glass are as follows. All the graphene samples were n-type and average sheet carrier concentration ( $n_{\text{sheet}}$ ) was  $3.3 \pm 0.5 \times 10^{15} \text{ 1/cm}^2$ . An average Hall mobility ( $\mu$ ) was estimated to be  $517 \pm 52 \text{ cm}^2/\text{Vs}$ . The average  $R_{\text{sheet}}$  was  $3.4 \pm 0.6 \text{ }\Omega/\text{sq}$ . The  $T$  of all the graphene films was almost 0%, which might indicate the number of layers of graphene was 400 layers and more.

The Raman spectrum of multilayer graphene film on glass is shown in (Fig. S3). The single and sharp (FWHM:  $15 \text{ cm}^{-1}$ ) G-band peak at  $1578 \text{ cm}^{-1}$  and absence of D-band peak at around  $1350 \text{ cm}^{-1}$  (deriving from defects or disorder) indicated that the graphene films were of high quality even after transfer. The shape of the 2D band peak at around  $2700 \text{ cm}^{-1}$  was similar to that of

graphite, indicating that the grown graphene films were very thick.

The SEM images of metal meshes are shown in (Fig. 2). Periodic mesh structures were observed for all samples. The design of each meshes from the definition of the mesh size is summarized in Table 1. It was found that the measured transmittance value well matches the calculated aperture ratio.

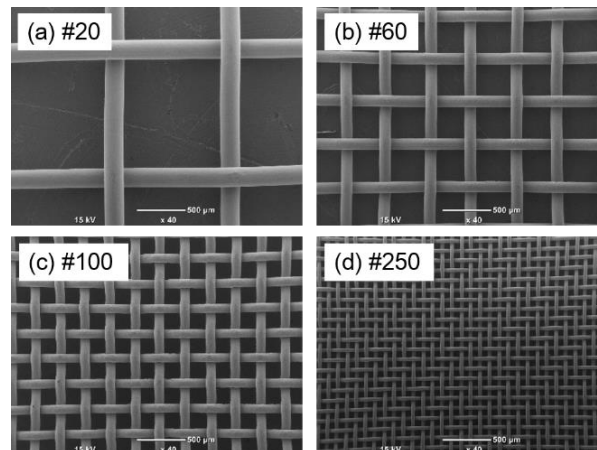


Fig. 2. The SEM images of metal meshes.

Table 1. Design of metal meshes.

Mesh#	Line width (mm)	Pitch (mm)	Aperture ratio (%)	$T@1200\text{nm}$ (%)
#20	0.20	1.10	71.2	$72.5 \pm 0.3$
#60	0.12	0.32	52.9	$52.1 \pm 0.1$
#100	0.095	0.16	39.8	$37.7 \pm 0.1$
#250	0.040	0.063	37.6	$33.6 \pm 0.1$

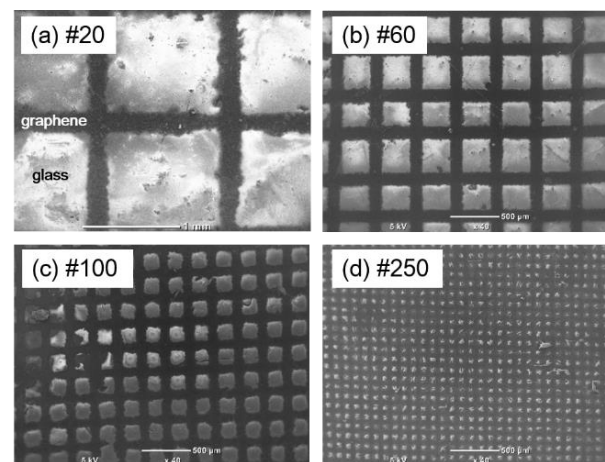


Fig. 3. The SEM images of graphene micromesh.

Fig. 3 shows the SEM images of graphene films after etching using each masks (graphene micromesh). It is obvious that the etched graphene films almost reflects the shape of the mesh mask. However edge of the patterned graphene was not smooth and needed to be optimized the etching conditions more. Physical properties of graphene micromesh were summarized in Table 2. The both of the line width

and pitch were almost same as those of metal meshes, respectively. The  $T$  of the graphene micromesh was lower than that of the metal mesh respectively. Although the  $T$  increases substantially in proportion to the aperture ratio, the  $R_{sheet}$  did not change drastically by changing the size of mesh as shown in (Fig. 4). The  $R_{sheet}$  of original graphene was about  $3.4 \pm 0.6 \Omega/sq$ , but it increased to about 20 - 30  $\Omega/sq$  after etching. In the sample #20, the etching conditions could not be optimized and the resistance was too high to measure. The best performance of graphene micromesh based transparent conductive films so far was  $R_{sheet} = 22.2 \Omega/sq$ . at  $T = 47.1 \pm 1.9 \%$ .

Table 2. Physical properties of graphene micromesh.

Mesh#	Line width (mm)	Pitch (mm)	T@1200nm (%)	$R_{sheet}$ ( $\Omega/sq.$ )
#20	0.20	1.10	54.6±6.9	N/A
#60	0.14	0.31	47.1±1.9	22.2
#100	0.10	0.15	29.7±2.2	23.3
#250	0.048	0.053	26.5±1.8	28.4

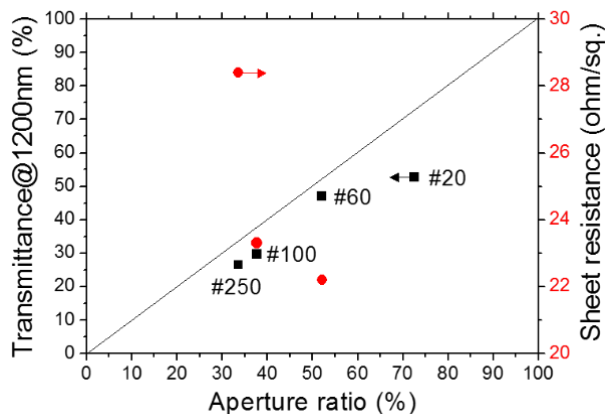


Fig. 4. Transmittance and sheet resistance of graphene micromesh.

We analyzed theoretically by considering the resistance of the graphene micromesh as the combined resistance of the two-dimensional resistance lattice circuit as shown in (Fig. 5). The combined resistance ( $R_{mn}$ ) between A (0, 0) and B (m, n) can be written as follows [21];

$$R_{mn} \sim \frac{\rho}{\pi W t} \left( \gamma + \frac{3}{2} \log 2 + \log \sqrt{m^2 + n^2} \right) \quad (1)$$

where  $\rho$  is resistivity of graphene ( $3.0 \times 10^{-5} \Omega \cdot cm$ ),  $t$  is thickness of graphene (120 nm),  $\gamma$  is Euler's constant ( $\sim 0.577$ ), and  $P/W$  is the ratio of pitch and line width. The  $P/W$  ratio depends on size of metal mesh. (Fig. 6) shows the measured and calculated combined resistance of graphene micromesh. According to theoretical calculations, if mesh number is fixed to 100 and a mesh with  $P/W = 18.5$  is used, a combined resistance of 46.8  $\Omega$  can be realized at  $T = 90\%$ . Such performance can be said to be sufficient for applying transparent conductive film of solar cell.

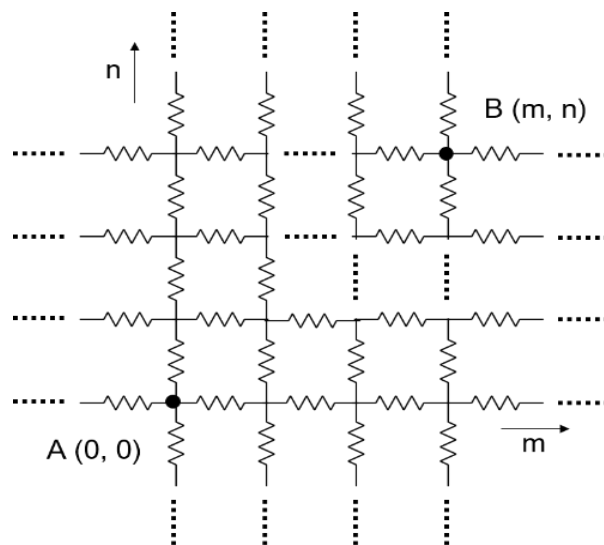


Fig. 5. Two-dimensional resistance lattice circuit.

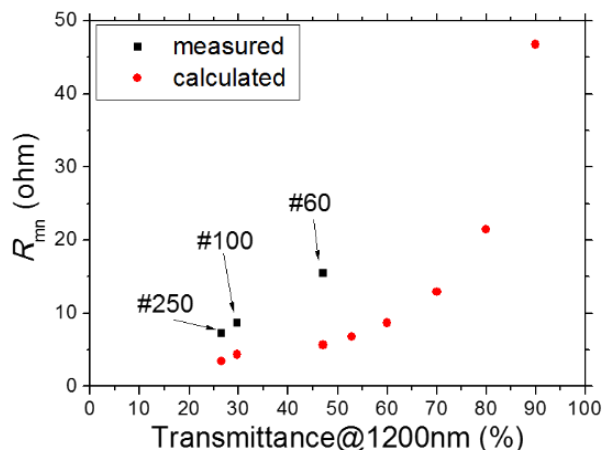


Fig. 6. The measured and calculated combined resistance.

### Conclusion

First of all, the CVD growth conditions of high quality multilayer graphene samples consisting of 400 layers or more were found using Ni foil, and the  $R_{sheet} = 3.4 \pm 0.6 \Omega/sq.$  was achieved. We succeeded in fabrication of graphene micromesh by  $O_2$  plasma using metal mesh mask. The best performance of graphene micromesh based transparent conductive films so far was  $R_{sheet} = 22.2 \Omega/sq.$  at  $T = 47.1 \pm 1.9 \%$ . According to theoretical calculations based on combined resistance of the two-dimensional resistance lattice circuit, a combined resistance of 46.8  $\Omega$  can be realized at  $T = 90\%$ . By designing the mesh masks based on the theoretical prediction and further optimizing the plasma etching conditions, we will further accelerate the improvement of properties of graphene micromesh and apply it to next generation solar cells and other devices.

### Acknowledgements

This work was supported by JST-ALCA program and JSPS-KAKENHI (grant numbers JP16K18356).

### Author's contributions

Conceived the plan: Ryouzuke Ishikawa, Nozomu Tsuboi; Performed the experiments: Hiroki Nishida, Hiro Fukushima, Sho Watanabe, Sohei Yamazaki, Gilgu Oh; Data analysis: Hiroki Nishida, Ryouzuke Ishikawa; Wrote the paper: Ryouzuke Ishikawa, Hiroki Nishida. Authors have no competing financial interests.

### Supporting information

Supporting informations are available from VBRI Press.

### References

1. Koh, W. S.; Gan, C. H.; Phua, W. K.; Akimov, Y. A.; Bai, P., *IEEE J. Sel. Top. Quantum Electron.* **2014**, 20.
2. Wang, X.; Zhi, L. J.; Mullen, K., *Nano Lett.*, **2008**, 8, 323.
3. Ishikawa, R.; Kurokawa, Y.; Miyajima, S.; Konagai, M., *Appl. Phys. Express*, **2017**, 10, 082301.
4. Ishikawa, R.; Ko, P. J.; Bando, M.; Kurokawa, Y.; Sandhu, A.; Konagai, M., *Nanoscale Res. Lett.*, **2013**, 8, 534.
5. Kim, D.; Lee, D.; Lee, Y.; Jeon, D. Y., *Adv. Funct. Mater.*, **2013**, 23, 5049.
6. Chen, Z. Y. et al.; *Appl. Phys. Lett.*, **2010**, 96.
7. Ishikawa, R.; Watanabe, S.; Nishida, H.; Aoyama, Y.; Oya, T.; Nomoto, T.; Tsuboi, N.; *Appl. Phys. Express*, **2018**, 11, 045101.
8. Kurokawa, Y.; Miyajima, S.; Yamada, A.; Konagai, M.; *Jpn. J. Appl. Phys.*, **2006**, 45, L1064.
9. Ishikawa, R.; Kato, S.; Yamazaki, T.; Kurokawa, Y.; Miyajima, S.; Konagai, M., *Jpn. J. Appl. Phys.*, **2014**, 53, 02BE09.
10. Siochi, E. J., *Nat. Nanotechnol.*, **2014**, 9, 745.
11. Iwase, A.; Ng, Y. H.; Ishiguro, Y.; Kudo, A.; Amal, R., *J. Am. Chem. Soc.*, **2011**, 133, 11054.
12. Kim, K. S. et al.; *Nature*, **2009**, 457, 706.
13. Hofmann, M.; Hsieh, Y. P.; Hsu, A. L.; Kong, J., *Nanoscale*, **2014**, 6, 289.
14. Yong, K.; Ashraf, A.; Kang, P.; Nam, S., *Sci. Rep.*, **2016**, 6.
15. Bai, J.; Zhong, X.; Jiang, S.; Huang, Y.; Duan, X., *Nat. Nanotechnol.*, **2010**, 5, 190.
16. Childres, I.; Jauregui, L. A.; Tian, J. F.; Chen, Y. P., *New J. Phys.* **2011**, 13.
17. Kim, Y. S. et al.; *Nanoscale* **2014**, 6, 10100-10105.
18. Dey, A.; Chroneos, A.; Braithwaite, N. S.; Gandhiraman, R. P.; Krishnamurthy, S., *Appl. Phys. Rev.*, **2016**, 3.
19. Chae, S. J. et al., *Adv. Mater.*, **2009**, 21, 2328.
20. Li, X. S. et al., *Nano Lett.*, **2009**, 9, 4359.
21. S. M. Sze. *WILEY-VCH* **2002**.